

Testing the Hubble Law with the *IRAS* 1.2 Jy Redshift Survey

Daniel M. Koranyi

Center for Astrophysics, 60 Garden St., Cambridge, MA 02138

and

Michael A. Strauss^{1,2}

Institute for Advanced Study, Princeton, NJ 08540

ABSTRACT

We test and reject the claim of Segal *et al.* (1993) that the correlation of redshifts and flux densities in a complete sample of *IRAS* galaxies favors a quadratic redshift-distance relation over the linear Hubble law. This is done, in effect, by treating the entire galaxy luminosity function as derived from the 60- μ m 1.2 Jy *IRAS* redshift survey of Fisher *et al.* (1995) as a distance indicator; equivalently, we compare the flux density distribution of galaxies as a function of redshift with predictions under different redshift-distance cosmologies, under the assumption of a universal luminosity function. This method does not assume a uniform distribution of galaxies in space. We find that this test has rather weak discriminatory power, as argued by Petrosian (1993), and the differences between models are not as stark as one might expect *a priori*. Even so, we find that the Hubble law is indeed more strongly supported by the analysis than is the quadratic redshift-distance relation. We identify a bias in the the Segal *et al.* determination of the luminosity function, which could lead one to mistakenly favor the quadratic redshift-distance law. We also present several complementary analyses of the density field of the sample; the galaxy density field is found to be close to homogeneous on large scales if the Hubble law is assumed, while this is not the case with the quadratic redshift-distance relation.

Subject headings:

1. Introduction

While the precise value of the Hubble constant H_0 is still the subject of controversy (cf. Jacoby *et al.* 1992), the linearity of the redshift-distance relation is generally not questioned by

¹Current address: Dept. of Astrophysical Sciences, Princeton University, Princeton, NJ 08544

²Alfred P. Sloan Foundation Fellow

most astronomers. Since its original announcement by Hubble (1929), observational evidence has mounted steadily in its favor; for recent discussions, see Lauer & Postman (1992), Peebles (1993), Riess, Press, & Kirshner (1996), and Perlmutter *et al.* (1996). However, Segal and collaborators have persistently argued for a quadratic redshift-distance relation wherein $z \propto r^p$, where z is the redshift, r is the distance, and $p = 2$ (Segal *et al.* 1993, hereafter SNWZ; Segal & Nicoll 1995, and references therein). This relation is predicted for the low-redshift regime in the Chronometric Cosmology developed by Segal (1976).

The greatest difficulty both in establishing the Hubble Law and in measuring H_0 is determining the distances to astronomical objects; this is often accomplished through the use of standard candles. The approach of Segal and collaborators in effect is to use the entire luminosity function of galaxies as a standard candle. If one assumes that the luminosity function of galaxies is independent of position and local density, at least after averaging over solid angle in a large redshift survey, then the comparison of the derived luminosity function as a function of redshift in principle could be a test of the assumed redshift-distance relation. Equivalently, the distribution of apparent magnitudes as a function of redshift in principle contains information about the redshift-distance relation (but see Petrosian 1993 and below). SNWZ choose to examine low-order statistics from the observed distribution of apparent magnitudes m and redshifts z in a given sample. In particular, they calculate the scatter in m , and the slope of the regression of magnitude on log redshift, comparing the expected values (under the assumption of various values of p) to what is actually observed. The distribution of apparent magnitudes or flux densities at a given redshift is independent of the density distribution of galaxies, and makes no assumption about the large-scale homogeneity of the universe. SNWZ have carried out this analysis using the 1.936 Jy redshift survey of galaxies observed with the *Infrared Astronomical Satellite (IRAS)* of Strauss *et al.* (1990; 1992). They found that $p = 1$ (the Hubble law) was strongly rejected by their analysis, with $p = 2$ (the Lundmark (1925) law) reproducing the observed magnitude-redshift correlations.

Despite the importance of Segal’s claims over the years, there has been very little response in the literature to this work. Soneira (1979) calculated the quantity $\langle z|m \rangle$ for the galaxies in the *Reference Catalogue of Bright Galaxies* (de Vaucouleurs & de Vaucouleurs 1964) and found that $p = 1$ was greatly favored by the data. However, this analysis requires the assumption of a homogeneous galaxy distribution, unlike the analysis of SNWZ (cf., Nicoll & Segal 1982). A similar analysis has been carried out by Shanks, as quoted in Peebles (1993, §5); see also Chołoniewski (1995). A more general discussion of the consequences of the quadratic redshift-distance law is given in Salpeter & Hoffman (1986). Finally, recent comparisons of observational data with the predictions of Chronometric Cosmology at high redshift (which we do *not* address in this paper) can be found in Segal & Nicoll (1986), Wright (1987; cf., Segal 1987), Cohen *et al.* (1988; cf., Segal 1990), Efron & Petrosian (1992), and Segal & Nicoll (1996).

Petrosian (1993) argues that given flux densities and redshifts for a complete sample, it is impossible to separate cosmological effects (including evolution) from the luminosity function; one must make additional assumptions about underlying distributions. He therefore argues that one

cannot use the observed correlations between flux density and redshift as a test of cosmologies. The results of this paper are in accord with this; we find that without additional assumptions about the underlying density field, the tests carried out by Segal are only very weak discriminants of cosmological models.

In the present paper, we carry out an analysis similar to that of SNWZ, using data from a redshift survey of *IRAS* galaxies. We discuss the derivation of the universal luminosity function in §2. In §3.1, we follow SNWZ in using the distribution of redshift and flux density as a function of redshift as a test of cosmological model. In §3.2, we allow ourselves the assumption that the galaxy distribution is homogeneous on large scales, giving us a variety of further cosmological tests. We conclude in §4.

2. Derivation of the Luminosity Function

The luminosity function $\Phi(L)$ of galaxies is the distribution of galaxies as a function of luminosity: $\Phi(L) dL$ is the mean number of galaxies per unit volume, with luminosity between L and $L + dL$. We will convert from redshift to distance by writing $cz = h_p r^p$, and arbitrarily adopt values of $h_p = 100 \text{ km s}^{-1} \text{ Mpc}^{-p}$. With these conventions, the luminosity L of a galaxy is given by $L = 4\pi(cz/h_p)^{2/p} \nu f$, where f is the observed flux density at frequency ν .

Following the notation of Yahil *et al.* (1991) we will find it useful to define the cumulative luminosity function $\Psi(L)$:

$$\Psi(L) = \int_L^\infty \Phi(L') dL' \quad , \quad (1)$$

implying that

$$\Phi(L) = -\frac{d\Psi}{dL} \quad . \quad (2)$$

The cumulative luminosity function is closely related to the selection function $\phi(z)$, which is the fraction of the luminosity function which enters the sample at a given redshift. For a sample that is flux-density-limited to $f \geq f_{min}$, we have

$$\phi(z) = \frac{\Psi[L_{min}(z)]}{\Psi[L_{min}(z_s)]} \quad , \quad (3)$$

where

$$L_{min} \equiv 4\pi(cz/h_p)^{2/p} \nu f_{min} \quad (4)$$

is the minimum luminosity detectable at redshift z , and $L_{min}(z_s)$ is a self-imposed lower limit on luminosity, corresponding to that of a galaxy at the flux density limit placed at $cz_s = 500 \text{ km s}^{-1}$.

Methods for deriving luminosity functions are reviewed by Binggeli, Sandage, & Tammann (1988) and by Strauss & Willick (1995), and can be classified as parametric or non-parametric. The former assume some implicit functional form for the luminosity function, characterized by a

number of parameters which are adjusted to provide the best fit to the observational data. The latter make no assumptions as to the form of the luminosity function, and are constructed directly from the data. However, both approaches assume that the luminosity function is universal; that is, independent of position or local density. This assumption of universality is of course a necessary one if we wish to use the observed luminosity distribution for cosmological tests (although, as Petrosian 1993 argues, and as we show below, it is not sufficient).

Here we will derive the luminosity function by maximum-likelihood estimation, following Nicoll & Segal (1978; 1980), Sandage, Tammann, & Yahil (1979), Nicoll & Segal (1983), Efstathiou, Ellis, & Peterson (1988), and Yahil *et al.* (1991). If the luminosity function is universal, then the joint probability density that we have a galaxy of luminosity L_i with redshift z_i is a separable function of these two variables:

$$\mathcal{F}(L_i, z_i) dL dz = \Phi(L_i)\rho(z_i) dL dz \quad , \quad (5)$$

where $\rho(z)$ is the local density of galaxies at redshift z . The conditional probability density $\mathcal{F}(L_i|z_i)$ that the galaxy have luminosity L_i , given its redshift z_i , is then given by the joint probability, divided by the integral of the joint probability over all possible luminosities in the sample at that redshift, given the flux density limit. That is,

$$\mathcal{F}(L_i|z_i) = \frac{\mathcal{F}(L_i, z_i)}{\int_{L_{min}(z_i)}^{\infty} \mathcal{F}(L, z_i) dL} = \frac{\Phi(L_i)}{\int_{L_{min}(z_i)}^{\infty} \Phi(L) dL} \quad . \quad (6)$$

Note that the density field $\rho(z)$ has dropped out of this equation. The quantity L_{min} is defined in Eq. (4); the p -dependence enters the analysis when calculating the luminosity of each galaxy from its redshift and flux density.

We then maximize the likelihood of observing the entire sample:

$$\mathcal{L} = \prod_i \mathcal{F}(L_i|z_i) \quad . \quad (7)$$

For computational convenience, we instead *minimize* the *negative logarithm* of the likelihood, where

$$-\ln \mathcal{L} = -\sum_i \ln \mathcal{F}(L_i|z_i) \quad . \quad (8)$$

An attempt was made to include p as one of the parameters with respect to which \mathcal{L} was maximized, but this proved impossible; \mathcal{L} turns out to be a monotonically increasing function of p .

The maximum-likelihood approach does not depend on the assumption that galaxies are distributed uniformly, since $\rho(z)$ dropped out of Eq. (6). However, this requires that the mean spatial density of galaxies in the sample be calculated by other means. There is a variety of such density estimators available (Davis & Huchra 1982); the one chosen here is

$$n_1 \equiv \Psi [L_{min}(z_s)] = V^{-1} \sum_i \frac{1}{\phi(z_i)} \quad , \quad (9)$$

where the sum is over all galaxies in the sample volume V , and $\phi(z_i)$ is the value of the selection function at the redshift of the i^{th} galaxy, as in Eq. (3).

The data set consists of 5313 pairs of 60 μm *IRAS* flux densities and redshifts above a flux density limit of 1.2 Jy, taken from Strauss *et al.* (1992) and Fisher *et al.* (1995). The recession velocities are corrected for the motion of the Sun with respect to the barycenter of the Local Group following Yahil, Tammann, & Sandage (1977). Of these galaxies, 4218 have redshifts in the range $500 \leq cz \leq 12000 \text{ km s}^{-1}$; only these were used in fitting the luminosity function since the sample may be incomplete at much higher redshifts (Fisher *et al.* 1992), and at low redshifts the local motions are strongly affected by peculiar velocities that dominate the local Hubble expansion.

2.1. Parameterized derivation

Various parameterizations of the luminosity function are discussed by Strauss (1989) and Saunders *et al.* (1990). We follow Yahil *et al.* (1991), in parameterizing the cumulative luminosity function by

$$\Psi(L) = C \left(\frac{L}{L_*} \right)^{-\alpha} \left(1 + \frac{L}{L_*} \right)^{-\beta} \quad , \quad (10)$$

so that the differential luminosity function is given by

$$\Phi(L) = -\frac{d\Psi(L)}{dL} = \left(\frac{\alpha}{L} + \frac{\beta}{L_* + L} \right) \Psi(L) \quad , \quad (11)$$

and the minimization is performed with respect to the two dimensionless parameters α and β and the characteristic luminosity L_* , using the routine `mrqmin` from Press *et al.* (1992). The optimal values of the parameters for $p = 1, 2, 3$ are tabulated in Table 1; the case $p = 3$ will be included in some of the tests we present for methodological perspective.

For graphical purposes, it is often convenient to work with the distribution per volume per *log* luminosity, given by

$$\hat{\Phi}(L) \equiv -\frac{d\Psi}{d(\log_{10}L)} = \frac{1}{\log_{10}e} L\Phi(L) \quad . \quad (12)$$

We shall use this form in making plots of the luminosity function.

2.2. Non-parameterized derivation

One drawback of assuming a parameterized form of the luminosity function is that it constrains the luminosity function to have a certain functional form, which may not be general enough to accurately reflect the actual luminosity function. A non-parametric approach to determining the luminosity function does not suffer from this limitation.

We model the differential luminosity function as being piecewise-constant over n bins evenly spaced in $\log_{10} L$ from the minimum to maximum luminosities seen in the sample, and then treat the value of the function on these bins as the n parameters with respect to which the likelihood (defined exactly as before) is to be maximized. This avoids any implicit assumptions of the functional form that the luminosity function should have, but also sacrifices any requirements as to continuity and smoothness that physical intuition suggests should be satisfied. This approach was first suggested by Nicoll & Segal (1980; 1983), and was reinvented by Efstathiou *et al.* (1988). Rather than attempting to search for a minimum in some high n -dimensional parameter space, the technique is to converge iteratively to the optimal step values. The interested reader is referred to the Appendix or Efstathiou *et al.* (1988) for details.

There are several drawbacks to the non-parametric luminosity function method. The most obvious is that the resultant luminosity function is discontinuous; this can be overcome by interpolating linearly between the centers of the bins; the details are set forth in the Appendix. We in fact use this interpolating method in what follows below. More serious is the effect illustrated below; a strong sensitivity of the derived luminosity function to bin size.

The ROBUST method of SNWZ calculates the luminosity function in two steps. For a given sample with maximum redshift z_{max} , there is a luminosity $L_{min}(z_{max}) = 4\pi (cz_{max}/h_p)^{2/p} \nu f_{min}$ above which a galaxy can be found anywhere in the volume of the survey, so $\Phi(L)$ in this luminosity range is simply proportional to the number of galaxies at each value of L . For lower luminosities, however, the volume in which a galaxy could be found is an increasing function of the luminosity, requiring further calculation to determine the luminosity function. Nicoll & Segal (1983) and SNWZ argue that the number of bins n_{ll} used *in the lower-luminosity range alone* should be set the same when comparing different cosmologies, in order to avoid giving any one cosmology extra degrees of freedom. Clearly, $n_{ll} < n$ by definition.

With this in mind, Figs. 1 and 2 show the resultant luminosity functions derived under the assumption of $p = 1$ and $p = 2$, respectively. We plot the parameterized luminosity function (Eq. 11, using the parameters of Table 1) as a solid curve, and superimpose the luminosity functions derived using the nonparametric method for several different binnings: the bin size used by SNWZ (in $\log L$), $n_{ll} = 10$ as recommended by SNWZ, and $n_{ll} = 25^3$. We plot error bars only for the non-parametric luminosity function that most closely approaches the parametric one. The bin sizes and number of bins for these and other luminosity functions are tabulated in Table 2 below. We also plot the luminosity functions of SNWZ for comparison (normalized using Eq. 9). Different bin sizes result in appreciable differences in the faint end of the luminosity function; in particular, the fewer the number of bins, the more the faint end of the luminosity function is attenuated.

³Because the range of luminosities below $L_{min}(z_{max})$ is dependent on the sample and the assumed value of z_{max} , our $n_{ll} = 10$ case has a different bin size than that of SNWZ.

At the bottom of these plots we have placed histograms indicating the distribution of the luminosities from which our luminosity functions were computed; note that the luminosity distribution of the galaxies in the sample narrows significantly with increasing p .

For $p = 1$, note that the luminosity function we find using the SNWZ binning is close to the luminosity function found by SNWZ themselves. However, this bin size is large enough to strongly bias the luminosity function at the faint end; the luminosity function does not become stable until the number of bins approaches $n = 20$ or more (corresponding to $n_{ll} = 15$). Thereafter, the luminosity function found by the non-parametric method, which is in principle free to assume any shape at all, is in good agreement with the parametric luminosity function. For $p = 2$, the sensitivity to binning seems to be much less severe, and the luminosity functions we find for all binnings are in very good agreement. In this case, we were able to reproduce the SNWZ luminosity function only with a very small number of bins $n_{ll} = 5$, corresponding to $n = 10$ (not shown).

The data set used by SNWZ consisted of the brighter half of the present one, flux density-limited at 1.936 Jy at 60 μm . This makes little difference; we find that the luminosity function from different subsets in flux density is quite robust (Koranyi 1993), as long as n_{ll} is large enough.

The biasing in the luminosity function due to binning is more severe for $p = 1$ than for $p = 2$, and therefore statistics for different values of p using these luminosity functions can give misleading results if the binning used is overly coarse. Indeed, we now show that with the bin size recommended by SNWZ, $p = 2$ is indeed a better fit to the data than is $p = 1$, while with finer binning, $p = 1$ is preferred.

3. Comparison of Different Cosmologies

Having derived a luminosity function for the sample under the assumption that the density and luminosity distributions of the sample are separable, we are now in a position to test the relative merits of the Hubble and Lundmark laws. We can test for robustness of the luminosity function, and also for self-consistency in the predictive powers of the luminosity function under the assumption of various power law cosmologies. These comparisons separate naturally into those that do and do not depend on the assumption that the galaxy distribution is uniform on large scales. We start with the latter, following SNWZ.

3.1. Density-independent comparisons

SNWZ argue strongly that it is important to distinguish between cosmological tests that involve quantities which depend on the cosmology itself (such as luminosity, or the luminosity function), and those that are pure observables (such as flux density, or equivalently magnitude, and redshift). Moreover, they develop statistical tests that do not depend on the assumption that

the distribution of galaxies is uniform in space. The statistics on which they put the greatest weight are s , the standard deviation of apparent magnitudes in a sample, and β , the slope of the regression of the apparent magnitudes on log redshift (the notation is that of SNWZ). Before calculating these statistics, it is useful to examine Fig. 3, which is the observed relation between apparent magnitudes (defined here, following SNWZ, as $m = 60 - 2.5 \log_{10} f$) and $\log_{10} cz$. The correlation between these two quantities is not very strong. The line shown is the regression line of m on $\log_{10} cz$ for the subsample of galaxies with $2000 < cz < 20,000 \text{ km s}^{-1}$; we have found that these statistics are very sensitive to the exact lower-redshift cutoff at redshifts below 2000 km s^{-1} . Table 2 gives the observed values of s and β . SNWZ calculate the expected values of these statistics using Monte-Carlo simulations. Here we will do so analytically.

Given a model for the luminosity function and a value of p , one can calculate the probability distribution function of flux density f of galaxy i , given its redshift z_i . The distribution function for a single galaxy is given by the luminosity function, normalized appropriately, following Eq. (6):

$$\mathcal{F}(f|z_i) = \frac{\frac{dL}{df} \Phi(L)}{\int_{L_{min}(z_i)}^{\infty} \Phi(L') dL'} \propto \frac{\Phi(L)}{\phi(z_i)} \quad , \quad (13)$$

where $\phi(z)$ is the selection function, $L = 4\pi\nu(cz_i/h_p)^{2/p} f$, and L_{min} was defined above in Eq. (4). From this distribution function, we can easily calculate the moments of the apparent magnitudes, and therefore the scatter s . Similarly, we can calculate the expectation value of m for each value of z , from which β follows directly. Note that both these statistics depend on the observed distribution of redshifts, and cannot be considered independent of this.

Table 2 shows the predicted results for $p = 1, 2$, and 3 for various binnings for the subsample of galaxies with $2000 < cz < 20,000 \text{ km s}^{-1}$. It is clear that the results are quite sensitive to the details of the binning. Let us start by concentrating on the results using the binning of SNWZ (the first row for each value of p). Both $p = 2$ and $p = 3$ do a much better job of predicting the observed apparent magnitude scatter s than does $p = 1$. We interpret this to be due to the fact that the $p = 1$ luminosity function is much more biased at this coarse binning than that of $p = 2$. We find similar results at $n_{ll} = 10$, as recommended by SNWZ. None of the models do a good job of reproducing the slope of regression, β , with this binning, with $p = 1$ overpredicting the observed value of β by as much as $p = 2$ underpredicts it. It is clear from Fig. 3, however, that a linear fit to the magnitude-log redshift scatter diagram is a rather poor way to model the data, and that the results may be quite sensitive to a small number of outlying points.

With finer binning ($n_{ll} = 25$), and with the parametrized luminosity function, the predictions for s are essentially *independent* of p . As Petrosian (1993) first argued, and as we conclude below, without additional assumptions, it is very difficult to distinguish cosmologies from redshift and magnitude data alone. However, note that the $p = 1$ does predict the correct value of β with this larger number of bins (the parametrized model does less well), while $p = 2$ and $p = 3$ fail quite badly. We describe the χ^2 column in this table below.

We can ask more of the data than simply these low-order statistics. Indeed, Eq. (13) gives a

prediction for the flux density distribution of galaxies as a function of redshift; we can compare this directly with what is observed. That is, the sum of these distribution functions over some subsample of a redshift survey can be compared with the *observed* flux density distribution as an *a posteriori* test of the luminosity function (Sandage *et al.* 1979; Yahil *et al.* 1991; Strauss & Willick 1995), or, in the present application, of the cosmology assumed. In other words, the predicted distribution of galaxies of a given flux density f is

$$N(f) = \sum_i \mathcal{F}(f|z_i) \quad , \quad (14)$$

where the summation is over all galaxies in a particular (sub)sample. The predicted and actual values in each bin can be compared with the χ^2 statistic, yielding a measure of how similar the two distributions in fact are.

Fig. 4 shows the results for the full sample of galaxies ($500 < cz < 20,000 \text{ km s}^{-1}$), as well as for a variety of redshift subsamples. The observed distribution in flux density is indicated by the dots, and the predictions for $p = 1$ and $p = 2$, using the luminosity functions with $n_{ll} = 25$ are indicated by the solid and dashed curves, respectively. As expected for a flux density-limited sample, the distributions peak strongly towards the flux density limit of 1.2 Jy, with a tail of higher flux density observations; since this must be the case regardless of cosmology, we are not surprised that there are no gross morphological differences between the flux density distributions for the competing cosmologies. Indeed, the difference between the predicted curves for $p = 1$ and $p = 2$ is very small. Following Yahil *et al.* (1991), we calculate the χ^2 statistic of the difference between the predicted and observed curves, using Poisson error bars and summing only over bins with five or more galaxies. The results are tabulated in Table 3. The fit with $p = 1$ is acceptable in all bins. $p = 2$ fares rather worse; although it is acceptable in several of the redshift bins, the fit for the full sample is unacceptable. For $p = 3$ (not shown in the figure) the fit in most redshift bins is unacceptable.

The quantity ν in Table 3 is the number of bins of flux density in which the comparison is done. One might argue that this number should be reduced by the number of free parameters in the luminosity function (25, in these cases!). We make two points here: first, we have found qualitatively very similar results to those presented here when we use the parameterized luminosity function of Eq. (11), which uses only three parameters (Table 1). Second, note that the fit to the luminosity function is done for galaxies with redshifts between 500 and 12,000 km s^{-1} ; for $p = 1$, this fit remains good for galaxies between 12,000 and 20,000 km s^{-1} , while for $p = 2$ and $p = 3$, the fit is unacceptable in this range.

Fig. 5 repeats this exercise using the SNWZ binning. The fits are not nearly as good as before, especially at the lowest luminosities. This is quantified in the χ^2 statistics tabulated in Table 4. However, although no value of p is acceptable, $p = 2$ is much preferred over $p = 1$, especially for the full sample. We saw in Figs. 1 and 2 that $n_{ll} = 10$ corresponds to a bin size which gives a strongly biased luminosity function for $p = 1$, but that the bias was much less severe for $p = 2$.

We explore the effect of binning further in Table 2. The χ^2 column gives the χ^2 values (for $\nu = 19$) for the flux density comparison for a variety of binnings, for the sample with $2000 < cz < 20,000 \text{ km s}^{-1}$. By this statistic, $p = 1$ is strongly ruled out with $n_{ll} = 10$ or with the SNWZ binning (doing much more poorly than even $p = 3$), while with either $n_{ll} = 25$ or with the parametrized luminosity function, $p = 1$ gives acceptable results.

We believe that this is the origin of the claims of SNWZ. With proper determination of the luminosity function, the distribution function of flux densities given the redshifts can be predicted almost as well with $p = 2$ as with $p = 1$; it is very insensitive to cosmology, as was pointed out originally by Petrosian (1993). However, the luminosity function is biased if one chooses too low a value of n_{ll} , and this effect is more severe for $p = 1$ than for $p = 2$, causing one to erroneously conclude that $p = 2$ is preferred by the data.

Our conclusion from this discussion, mirroring that of Petrosian (1993), is that *any* statistic derived from the distribution of flux densities and redshifts will be able to match the data roughly equally well for $p = 1$ or $p = 2$, without making further assumptions about the distributions.

One such assumption we could make is that the universe approaches homogeneity on the largest scales (the Cosmological Principle; cf., Peebles 1993). With such an assumption, we can derive further statistics that do allow a sharp distinction between different values of p .

3.2. Density-dependent comparisons

Under the homogeneous approximation, one can predict the distribution of galaxies with redshift, given the luminosity function and a value of p . In a shell of thickness Δz at a redshift z , one expects there to be

$$N(z) = \frac{\omega}{p} n_1 \phi(z) \left(\frac{cz}{h_p} \right)^{3/p-1} \Delta z \quad (15)$$

galaxies, where ω is the solid angle covered by the sample (11.06 ster in our case; cf. Strauss *et al.* 1990). These predictions for various p are shown in the upper panel of Fig. 6, along with the observed distribution with redshift (we use $n_{ll} = 25$ throughout this section). The lower panel shows the ratio of the observed to predicted counts (which is the fractional density of the shell relative to the mean over the sample). The $p = 1$ curve agrees closely with the observed distribution, although the agreement is not perfect. The effects of the Local Supercluster at $cz \simeq 1500 \text{ km s}^{-1}$ and of the Great Attractor and Pisces-Perseus regions at $cz \simeq 4500 \text{ km s}^{-1}$ are visible as overdensities, even when averaged over almost the entire sky. At very large redshifts, the $p = 1$ curve slightly overestimates the observed distribution, probably because of incompleteness of the sample at high redshifts (Fisher *et al.* 1992). However, if either the $p = 2$ or $p = 3$ model were correct, one would have to argue that as one looks to higher redshifts in the universe, the inhomogeneities grow. The galaxy density plotted in the lower panel would need to be a strong function of redshift: low nearby, rising rapidly to a maximum at $5000 - 10,000 \text{ km s}^{-1}$, and then

dropping by a factor of two thereafter. This would violate the Cosmological Principle, and indeed, if such massive structures were common in the universe, we would see them reflected in the angular correlation function of faint galaxies (*e.g.* Maddox *et al.* 1990).

Indeed, one can calculate the distribution of densities on shells as a function of redshift, without any calculation of the luminosity function at all (Saunders *et al.* 1990). In § 2 above, we calculated the distribution function of luminosities conditioned on the redshifts $\mathcal{F}(L_i|z_i)$. Here we calculate the distribution of redshifts conditioned on the luminosities $\mathcal{F}(z_i|L_i)$, which is given by:

$$\mathcal{F}(z_i|L_i) = \frac{\mathcal{F}(L_i, z_i)}{\int dz \frac{dV}{dz} \mathcal{F}(L_i, z)} = \frac{\rho(z_i)}{4\pi \int_0^{z_{max,i}} dz z^{3/p-1} \rho(z)} \quad , \quad (16)$$

where

$$z_{max,i} = \frac{h_p}{c} \left(\frac{L_i}{4\pi\nu f_{min}} \right)^{p/2} \quad . \quad (17)$$

When we conditioned on redshift (Eq. 6), the density distribution dropped out of the expression, while here, the luminosity function drops out. We can now maximize the likelihood with respect to the density field defined at a series of steps, exactly as we did with the luminosity function⁴, using the iterative technique described by Efstathiou *et al.* (1988). The results are shown as points in the lower panel of Fig. 6. The solid points are for $p = 1$, the open circles for $p = 2$, and the stars for $p = 3$. Error bars are given only for $p = 1$ to keep the figure from getting overly crowded; the error bars are in fact quite insensitive to the value of p . The agreement between this density field and that given by the curves, which depends on the calculation of the luminosity function, is striking; this shows us that both the luminosity function and density field calculations are robust.

A final approach is suggested by Soneira (1979) and Chołoniewski (1995); cf., Nicoll & Segal (1982). The expectation value of $\log z$ as a function of flux density follows directly from Eq. (16):

$$\langle \log z | f \rangle = \frac{\int dz \frac{dV}{dz} \log z \mathcal{F}(L, z)}{\int dz \frac{dV}{dz} \mathcal{F}(L, z)} = \frac{\int dz \log z z^{3/p-1} \rho(z) \Phi(L)}{\int dz z^{3/p-1} \rho(z) \Phi(L)} \quad , \quad (18)$$

where $L = 4\pi(cz/h_p)^{2/p}\nu f$. Unlike the expressions for the conditional probabilities, neither ρ nor Φ drops out of the expression. Fig. 7 shows this statistic in bins of \log flux density for the full *IRAS* sample (solid points, with errors in the mean shown) and also for the Northern and Southern Galactic hemispheres of the sample separately (open circles and stars, respectively), as a test of the robustness of the statistic to density inhomogeneities. The averaging is done for galaxies in the redshift range 500 km s^{-1} to $20,000 \text{ km s}^{-1}$. The $p = 1$ prediction assuming $\rho(z) = 1$ is given as the light solid line, while $p = 2$ is shown with the light dashed line. These curves are not pure power laws, because of the upper limit on redshift we imposed. The $p = 1$ line is not a perfect fit to the data; one is presumably seeing the residual effect of density inhomogeneities, as is made

⁴We will not, however, apply the additional complication of interpolating the density field between bins as we do in the Appendix for the luminosity function.

clear by the differences between the Northern and Southern hemispheres, especially at large flux densities. However, $p = 2$ does much more poorly, especially at large flux densities. This is not unexpected: as Fig. 6 showed, the homogeneity assumption is a very poor one for the $p = 2$ model. We can include this effect by carrying out the integration of Eq. (18), using the density field found non-parametrically in Fig. 6; the results are shown as the heavy solid and dashed line for $p = 1$ and $p = 2$, respectively. The $p = 1$ line is now in excellent agreement with the data, while the $p = 2$ line approaches the data points somewhat more closely, but is still far from a good fit to the data. It is not clear whether this represents a breakdown of the universal luminosity function assumption which went into Eq. (18), for the case of $p = 2$.

4. Conclusions

The density-dependent methods of comparing the cosmologies favor $p = 1$ quite unambiguously. However, one reaches this conclusion only with the auxiliary assumption that the density field of galaxies approaches homogeneity on large scales. In the case of the density-independent comparisons of the distribution of flux density, we have recourse to quantitative χ^2 testing of goodness-of-fit, and we find that the standard $p = 1$ cosmology yields better agreement than does the $p = 2$ case. But perhaps most surprising is the extent to which these methods do a poor job of discriminating between different values of p , implying that the results of any analysis predicated on their use should be interpreted with great caution. These results are in accord with the analytic arguments of Petrosian (1993): without additional assumptions, questions of cosmology and the appropriate luminosity function cannot be decoupled from flux density and redshift data, and that one cannot determine both simultaneously.

A further methodological pitfall which affects SNWZ is the sensitivity of the non-parametric luminosity function to bin size. SNWZ used very coarse binning and therefore were working with luminosity functions inaccurate at the faint end. Since this effect is less pronounced for $p = 2$ than for $p = 1$, the luminosity function that SNWZ employed for $p = 2$ was less in error than the one they employed for $p = 1$. We found that with equally coarse binning, this effect causes $p = 2$ to be favored, both by the statistics used by SNWZ and by our own comparisons of the flux density distribution.

Therefore from redshift survey data alone, one can conclude that $p = 1$ is preferred only weakly over $p = 2$ if we only allow ourselves the assumption of a universal luminosity function. When one makes the additional assumption that the distribution of galaxies approaches isotropy on large scales, the case for $p = 1$ becomes *much* stronger; indeed, if $p = 2$, one would need to argue that the density field of galaxies beyond 10,000 km s⁻¹ drops dramatically and steadily with redshift. When this is combined with the observed linearity of the redshift-distance diagram using measurements of extragalactic standard candles (cf., Mould *et al.* 1991; Lauer & Postman 1992; Hamuy *et al.* 1995, 1996; Perlmutter *et al.* 1996; Riess *et al.* 1996), the evidence for the Hubble law becomes overwhelming.

We thank Dr. I. Segal for detailed comments on an earlier draft of this paper, and Marc Davis for suggesting we include the Soneira (1979) statistic in this paper. D.M.K. was supported by a National Science Foundation Graduate Fellowship. M.A.S. acknowledges support from the W.M. Keck Foundation, NASA Theory Grant NAG5-2882, and the Alfred P. Sloan Foundation.

A. Interpolation of the piecewise-constant luminosity function

The piecewise-constant luminosity function as defined by Efstathiou *et al.* (1988) has one drawback; the corresponding selection function (defined from Eqs. 3 and 1) shows a scalloping effect (cf., Strauss & Koranyi 1994). This is illustrated in Fig. 8, which shows the ratio of the selection function calculated from the piecewise-constant luminosity function (dashed line) calculated with bins of $\Delta \log L = 0.15$, to the analytic selection function (from Eq. 10). These were calculated for $p = 1$. The selection function of the piecewise-continuous luminosity function has a discontinuity in slope at the edge of each bin (as indeed it must; the slope is proportional to the luminosity function itself). The effect is minimized here by using small bins, but nevertheless it would be best to eliminate this altogether. We do so by generalizing the method of Efstathiou *et al.* (1988) to define the luminosity function not as constant in a series of bins, but rather as a series of line segments connecting bins. The formalism of Efstathiou *et al.* can be carried over exactly, if we replace Equations 2.8-2.11 of that paper with the following. Define the luminosity function to be a series of line segments connecting a series of points $(L_k, \Phi_k), k = 1, \dots, n^5$; thus

$$\Phi(L) = \sum_{k=1}^n \Phi_k W(L, k) \quad . \quad (\text{A1})$$

Note that in the present paper, we refer to the luminosity function as Φ , while Efstathiou *et al.* refer to it as ϕ . The logarithm of the likelihood is then given by

$$\ln \mathcal{L} = \ln \left[\sum_{i=1}^N \sum_{k=1}^n \Phi_k W(L, k) \right] - \ln \left[\sum_{i=1}^N \sum_{k=1}^n \Phi_k [H(L_{min}(z_i), k) - H(L_{max}(z_i), k)] \right] \quad , \quad (\text{A2})$$

where N is the total number of galaxies in the sample. Note that Eq. (2.9) of Efstathiou *et al.* is erroneously missing the summation over k in the first term on the right-hand side. Here, L_{min} is defined in Eq. (4), and $L_{max}(z_i) = 4\pi(cz/h_p)^{2/p} \nu f_{max}$ if one derives the luminosity function for samples with an upper limit on flux density. If there is no upper limit on flux density, $H(L_{max}(z_i), k) = 0$.

The expressions for W and H are more complicated than those in Efstathiou *et al.* (1988),

⁵Unlike Nicoll & Segal (1983), we do not explicitly split our calculation of Φ into those regions above and below $L_{min}(z_{max})$. There is therefore no reference to n_U in this Appendix.

but they just involve linear interpolation:

$$W(L, k) = \begin{cases} \frac{L-L_{k-1}}{L_k-L_{k-1}} & L_{k-1} < L \leq L_k \text{ and } k \neq 1 \\ \frac{L_{k+1}-L}{L_{k+1}-L_k} & L_k < L \leq L_{k+1} \text{ and } k \neq n \\ 0 & \text{otherwise.} \end{cases} \quad (\text{A3})$$

$$H(L, k) = \begin{cases} \frac{1}{2}(L_{k+1} - L_{k-1}) & L \leq L_{k-1} \text{ and } k \neq 1 \\ \frac{1}{2} \left[L_{k+1} - L_k + (L_k + L - 2L_{k-1}) \frac{L_k - L}{L_k - L_{k-1}} \right] & L_{k-1} < L \leq L_k \text{ and } k \neq 1 \\ \frac{1}{2} \frac{(L_{k+1} - L)^2}{L_{k+1} - L_k} & L_k \leq L < L_{k+1} \text{ and } k \neq n \\ 0 & \text{otherwise.} \end{cases} \quad (\text{A4})$$

Note that here, we define $L_{n+1} \equiv L_n$. Finally, the integral constraint we use is:

$$\sum_k \Phi_k(L_k - L_{k-1}) = 1 \quad . \quad (\text{A5})$$

One can normalize after this using the quantity n_1 defined in Eq. (9) (as indeed we have done in Fig. 8). The solid line in Fig. 8 shows the ratio of selection function for the resulting continuous luminosity function to that for the analytic luminosity function; the scalloping effect has gone away. Other than the scalloping effect, the interpolated selection function, and that using the piece-wise continuous method are in good agreement, implying that this interpolation technique has very little effect on the derived luminosity function (although both differ at the 10% level from the analytic luminosity function; this is a residual effect of the finite binning, as described in §2). However, it does have a non-negligible effect on the derived selection function, and we have used it in all calculations requiring a nonparametric luminosity function in this paper.

Table 1. Parameters of the parameterized luminosity function.

p	α	β	$\log_{10}(L_*)$ L_{\odot}	n_1 $(10^{-6}(\text{km s}^{-1})^{-3/p})$
1	0.49 ± 0.07	1.81 ± 0.12	$9.68^{+0.10}_{-0.13}$	0.058
2	-0.02 ± 0.14	2.47 ± 0.14	$7.98^{+0.10}_{-0.13}$	4.357
3	-0.81 ± 0.30	3.07 ± 0.24	$7.16^{+0.10}_{-0.14}$	25.25

Table 2. Statistics of SNWZ for the sample with $2000 < cz < 20,000 \text{ km s}^{-1}$.

Model	n_l^a	n^b	$\Delta \log L^c$	s^d	β^e	χ^2^f	
Real data	—	—	—	0.628	0.610	—	
$p = 1$	9	13	0.365	0.686	0.700	377.7	Bin size used by SNWZ
$p = 1$	10	14	0.302	0.661	0.677	203.0	
$p = 1$	25	37	0.109	0.599	0.591	10.7	
$p = 1$	—	—	—	0.587	0.536	5.1	Parameterized Luminosity Function
$p = 2$	8	18	0.187	0.616	0.520	115.7	Bin size used by SNWZ
$p = 2$	10	21	0.137	0.604	0.489	73.0	
$p = 2$	25	53	0.052	0.592	0.452	40.4	
$p = 2$	—	—	—	0.588	0.444	38.9	Parameterized Luminosity Function
$p = 3$	7	22	0.131	0.613	0.369	103.9	Bin size used by SNWZ
$p = 3$	10	29	0.089	0.608	0.349	76.7	
$p = 3$	25	71	0.034	0.604	0.332	59.4	
$p = 3$	—	—	—	0.597	0.328	71.8	Parameterized Luminosity Function

^aThe number of bins in the luminosity function below $L_{min}(z_{max})$.

^bThe total number of bins in the luminosity function.

^cThe size of the bins in $\log L$.

^dThe standard deviation of the apparent magnitudes.

^eThe slope of the apparent magnitude regression on $\log cz$.

^fThe χ^2 of the predicted flux density distribution of the sample to that observed.

Table 3. χ^2 analysis for flux density distribution of galaxies, $n_{ll} = 25$.

cz km s ⁻¹	ν	# of Galaxies	χ^2	$p = 1$		$p = 2$		$p = 3$	
				χ^2/ν	χ^2	χ^2/ν	χ^2	χ^2/ν	
500–2000	19	674	23.1	1.21	22.0	1.16	39.8	2.09	
2000–4000	17	901	14.2	0.84	20.5	1.21	23.8	1.40	
4000–6000	15	1068	13.8	0.92	17.0	1.14	19.9	1.32	
6000–8000	13	697	18.5	1.42	26.4	2.03	32.1	2.47	
8000–12,000	11	878	5.0	0.46	8.6	0.78	17.6	1.60	
12,000–20,000	10	639	9.8	0.98	16.6	1.66	24.9	2.49	
Entire Sample	19	4857	12.2	0.64	45.7	2.40	70.4	3.70	

Table 4. χ^2 analysis for flux density distribution of galaxies, using SNWZ binning.

cz km s ⁻¹	ν	# of Galaxies	χ^2	$p = 1$		$p = 2$		$p = 3$	
				χ^2/ν	χ^2	χ^2/ν	χ^2	χ^2/ν	
500–2000	19	674	41.8	2.20	23.9	1.26	35.1	1.85	
2000–4000	17	901	84.8	4.99	31.2	1.84	25.1	1.48	
4000–6000	15	1068	119.7	7.98	33.9	2.26	25.7	1.71	
6000–8000	13	697	109.2	8.40	57.2	4.40	45.9	3.53	
8000–12,000	11	878	61.6	5.60	22.1	2.01	26.4	2.40	
12,000–20,000	10	639	19.5	1.95	19.6	1.96	28.2	2.82	
Entire Sample	19	4857	299.6	15.77	111.3	5.86	106.9	5.63	

REFERENCES

- Binggeli, B., Sandage, A. & Tammann, G.A. 1988, *ARA&A*, 26, 509
- Choloniewski, J. 1995, *MNRAS*, submitted (astro-ph 9504035)
- Cohen, M.H., Barthel, P.D., Pearson, T.J., & Zensus, J.A. 1988, *ApJ*, 329, 1
- Davis, M., & Huchra, J. P. 1982, *ApJ*, 254, 437
- de Vaucouleurs, G., & de Vaucouleurs, A. 1964, *Reference Catalogue of Bright Galaxies* (Austin: University of Texas Press)
- Efron, B., & Petrosian, V. 1992, *ApJ*, 399, 345
- Efstathiou, G., Ellis, R.S. & Peterson, B.A. 1988, *MNRAS*, 232, 431
- Fisher, K.B., Strauss, M.A., Davis, M., Yahil, A. & Huchra, J.P. 1992, *ApJ*, 389, 188
- Fisher, K.B., Huchra, J.P., Davis, M., Strauss, M.A., Yahil, A. & Schlegel, D. 1995, *ApJS*, 100, 69
- Hamuy, M., Phillips, M. M., Maza, J., Suntzeff, N., Schommer, R. A., & Aviles, R. 1995, *AJ*, 109, 1
- Hamuy, M., Phillips, M. M., Suntzeff, N., Schommer, R. A., Maza, J., & Aviles, R. 1996, *AJ*, in press (astro-ph/9609062)
- Hubble, E. 1929, *Proc. N.A.S.*, 15, 168
- Jacoby, G.H., Branch, D., Ciardullo, R., Davies, R.L., Harris, W.E., Pierce, M.J., Pritchett, C.J., Tonry, J.L. & Welch, D.L. 1992, *PASP*, 104, 599
- Koranyi, D.M. 1993, Senior Thesis, Princeton University
- Lauer, T.R. & Postman, M. 1992, *ApJ*, 400, L47
- Lundmark, K. 1925, *MNRAS*, 85, 865
- Maddox, S. J., Efstathiou, G., Sutherland, W. J., & Loveday, J. 1990, *MNRAS*, 242, 43P
- Mould, J. R. *et al.* 1991, *ApJ*, 383, 467
- Nicoll, J.F. & Segal, I.E. 1978, *Ann. Phys.*, 113, 1
- Nicoll, J.F. & Segal, I.E. 1980, *A&A*, 82, L3
- Nicoll, J.F. & Segal, I.E. 1982, *ApJ*, 258, 457
- Nicoll, J.F. & Segal, I.E. 1983, *A&A*, 118, 180

- Peebles, P.J.E. 1993, *Principles of Physical Cosmology* (Princeton: Princeton University Press)
- Perlmutter, S. *et al.* 1996, preprint (astro-ph/9608192)
- Petrosian, V. 1993, in *Statistical Challenges in Modern Astronomy*, edited by E.D. Feigelson & G.J. Babu (New York: Springer-Verlag), p. 173
- Press, W.H., Flannery, B.P., Teukolsky, S.A. & Vetterling, W.T. 1992 *Numerical Recipes in Fortran: The Art of Scientific Computing* (Cambridge: Cambridge University Press)
- Riess, A., Press, W., & Kirshner, R.P. 1996, preprint (astro-ph/9604143)
- Salpeter, E.E., & Hoffman, G.L. 1986, *Proc. N.A.S.*, 83, 3056
- Sandage, A., Tammann, G. A., & Yahil, A. 1979, *ApJ*, 232, 352
- Saunders, W., Rowan-Robinson, M., Lawrence, A., Efstathiou, G., Kaiser, N., Ellis, R.S., & Frenk, C.S. 1990, *MNRAS*, 242, 318
- Segal, I.E. 1976, *Mathematical Cosmology and Extragalactic Astronomy* (New York: Academic Press)
- Segal, I.E. 1987, *ApJ*, 320, 135
- Segal, I.E. 1990, *MNRAS*, 242, 423
- Segal, I.E. & Nicoll, J.F. 1986, *ApJ*, 300, 224
- Segal, I.E. & Nicoll, J.F. 1995, *Proc. N. A. S.*, submitted
- Segal, I.E. & Nicoll, J.F. 1996, *ApJ*, 459, 456
- Segal, I.E., Nicoll, J.F., Wu, P. & Zhou, Z. 1993, *ApJ*, 411, 465 (SNWZ)
- Soneira, R.M. 1979, *ApJ*, 230, L63
- Strauss, M.A. 1989, Ph.D. Thesis, University of California, Berkeley
- Strauss, M.A., Davis, M., Yahil, A. & Huchra, J.P. 1990, *ApJ*, 361, 49
- Strauss, M. A., Huchra, J. P., Davis, M., Yahil, A., Fisher, K. B., & Tonry, J. 1992, *ApJS*, 83, 29
- Strauss, M. A., & Koranyi, D. M. 1994, *Cosmic Velocity Fields*, edited by F.R. Bouchet and M. Lachièze-Rey (Gif sur Yvette: Editions Frontières), 581
- Strauss, M. A., & Willick, J. A. 1995, *Phys. Rep.*, 261, 271
- Wright, E.L. 1987, *ApJ*, 313, 551
- Yahil, A., Strauss, M.A., Davis, M. & Huchra, J.P. 1991, *ApJ*, 372, 380

Yahil, A., Tammann, G., & Sandage, A. 1977, ApJ, 217, 903

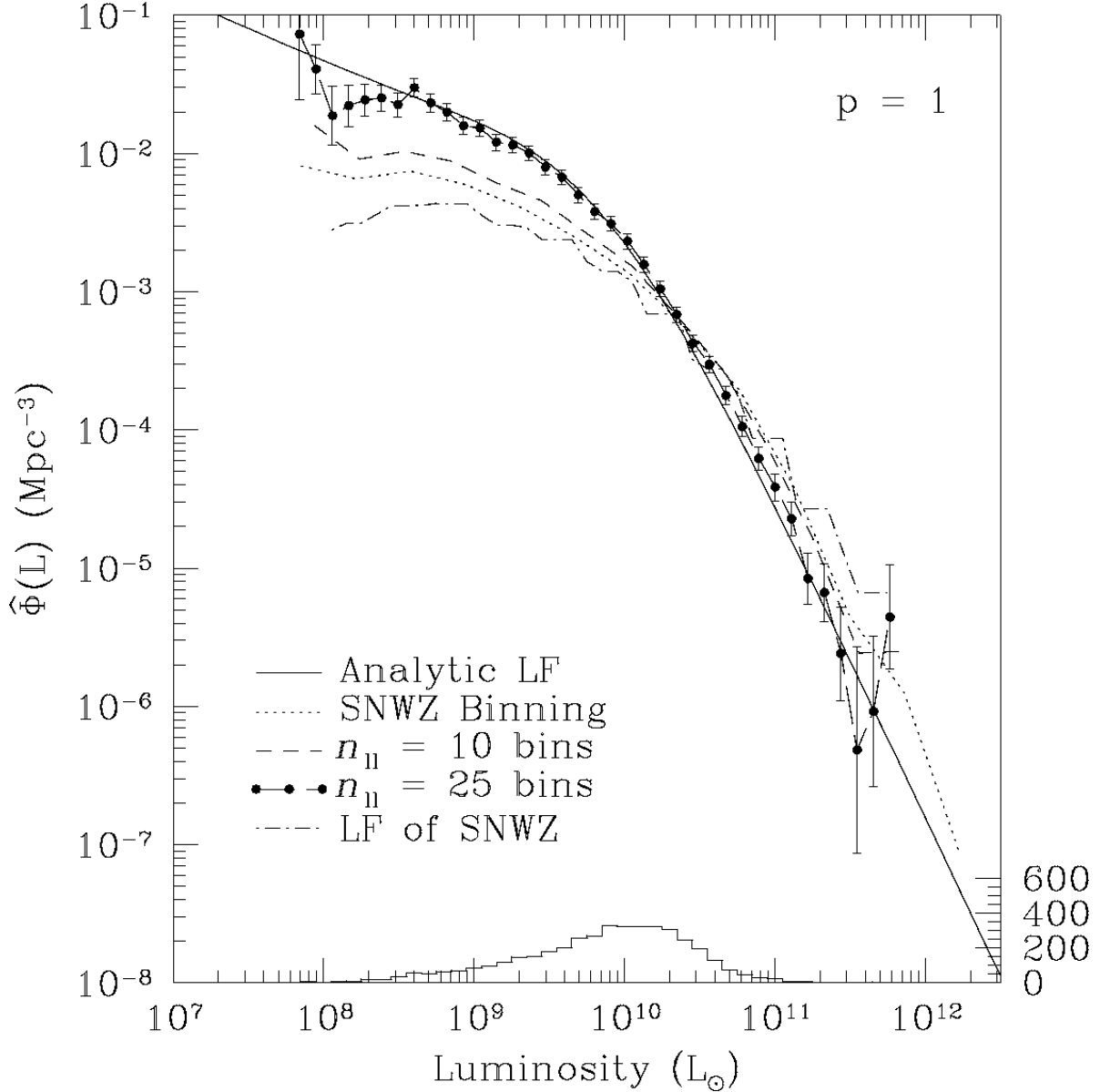


Fig. 1.— Plots of the luminosity function derived by both parametric and non-parametric methods for $p = 1$; the solid curve is parametric, and three non-parametric luminosity functions are shown, with different binning in $\log L$. Error bars are suppressed except for the luminosity function with the finest binning, which matches the parameterized luminosity function quite closely. The luminosity function of SNWZ is plotted for comparison. The histogram at the bottom indicates the luminosity distribution of the galaxies in the sample.

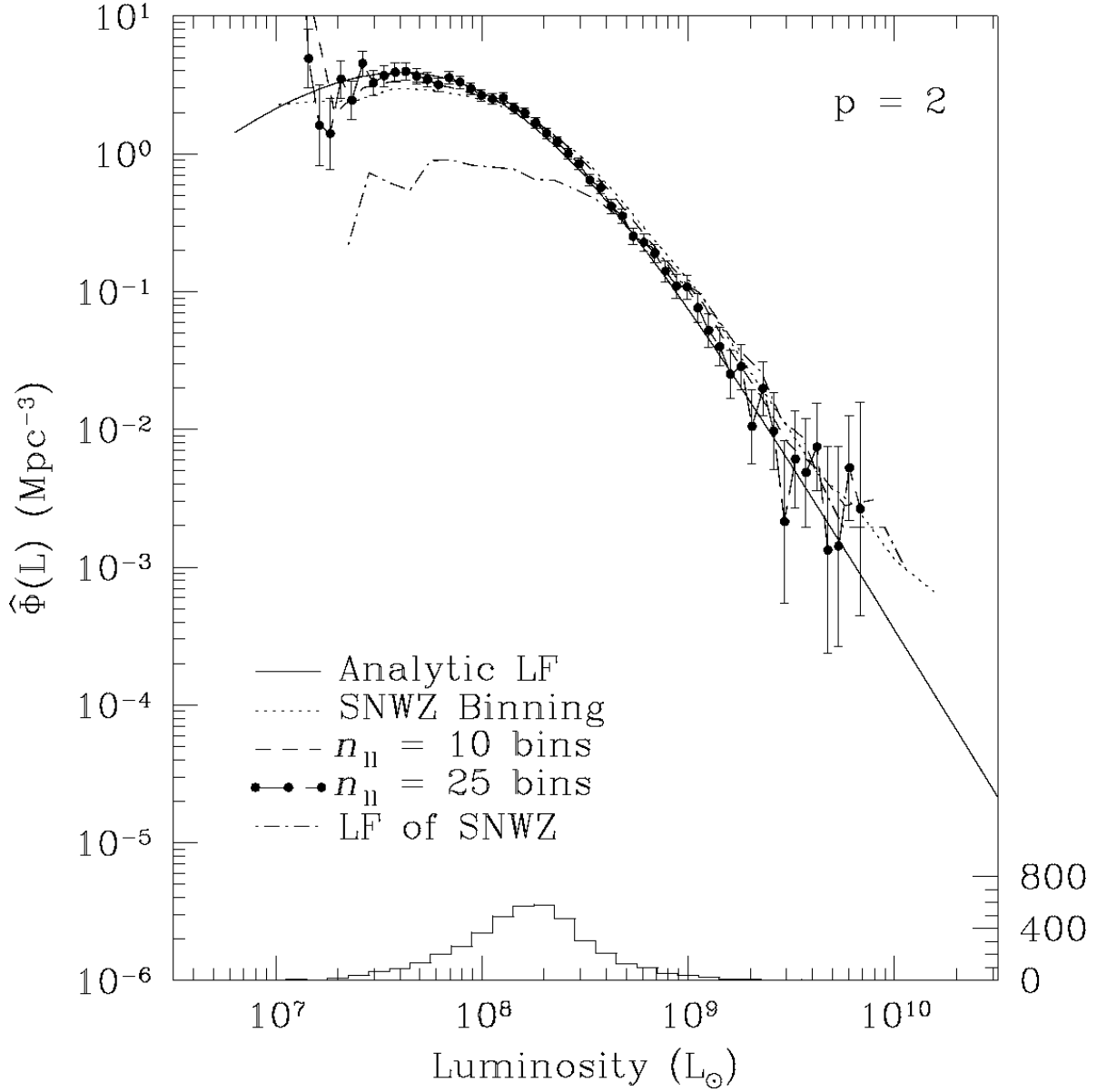


Fig. 2.— As in Fig. 1, but for $p = 2$.

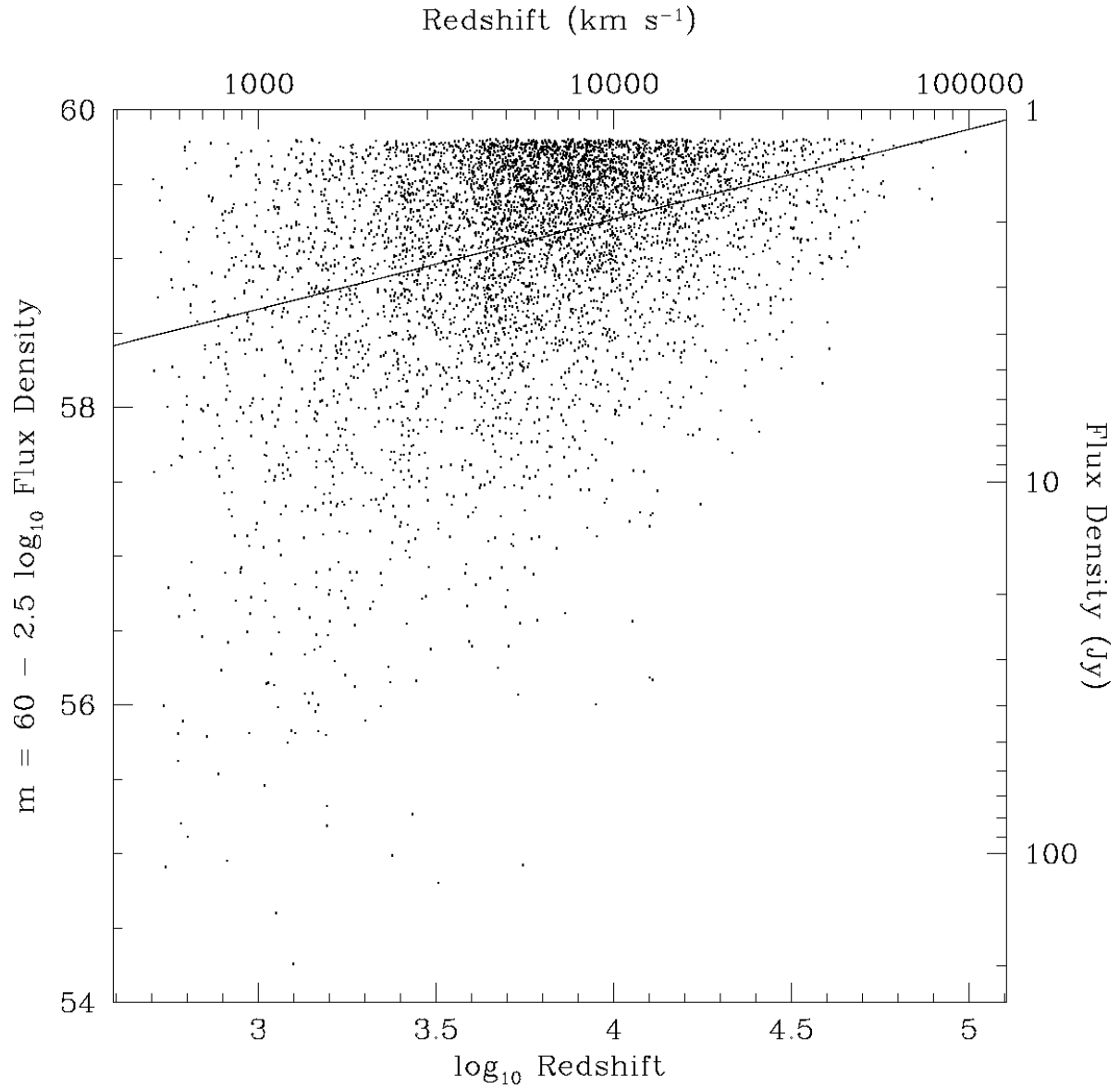


Fig. 3.— The observed distribution of apparent magnitudes m as a function of $\log_{10} cz$. The line is the best-fit regression for those galaxies with $2000 < cz < 20,000 \text{ km s}^{-1}$.

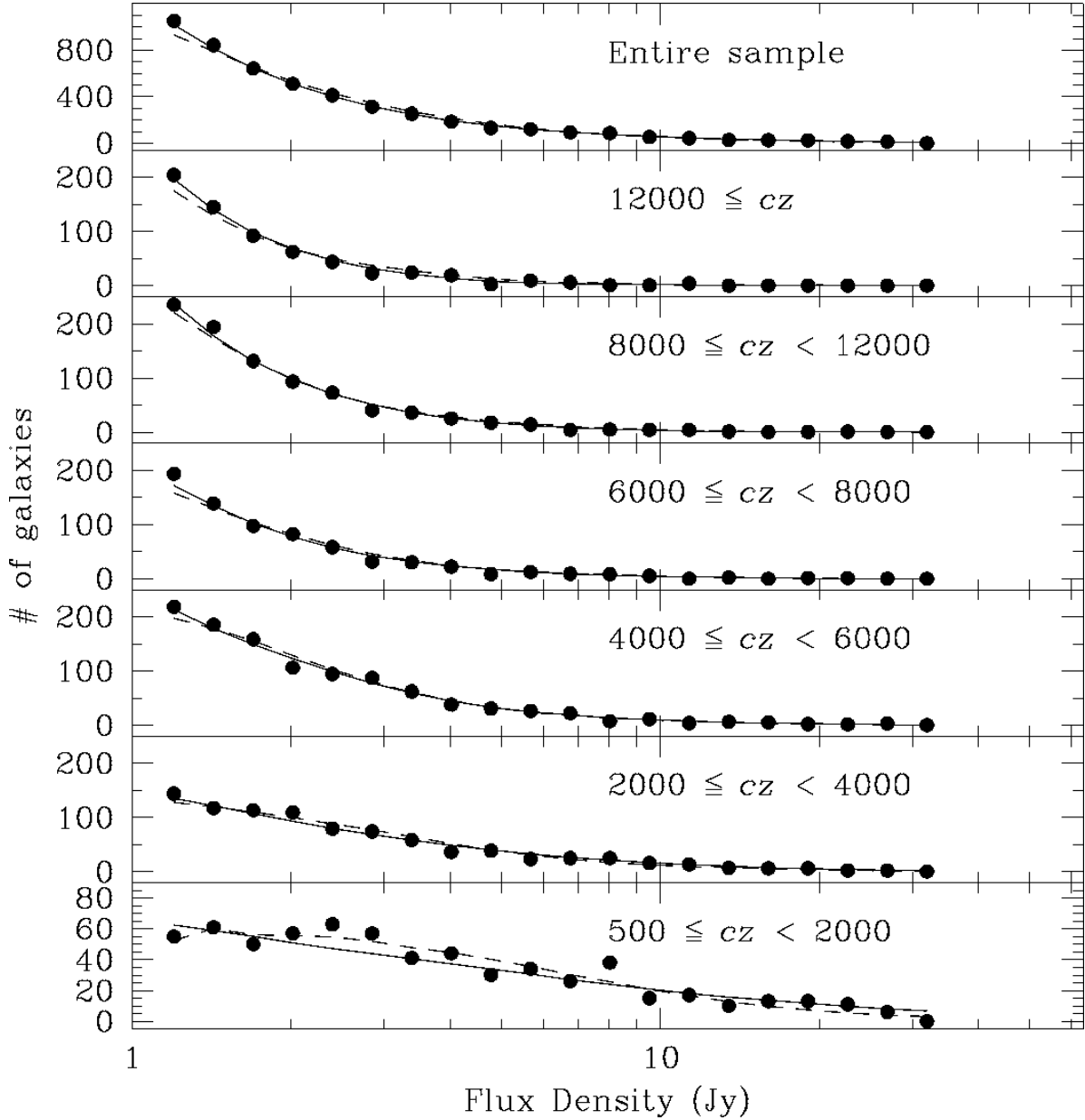


Fig. 4.— Observed (points) and expected (curves) distribution of galaxies in flux density at different redshift ranges (labeled in km s^{-1}). The solid curves are for $p = 1$, and the dashed curves for $p = 2$. Topmost box is for the entire sample. Note the virtual indistinguishability of the predictions for the two power laws; this shows that the flux density (or equivalently apparent magnitude) distribution has little discriminatory power. Predictions are based on the nonparametric luminosity function fitted over the range $500\text{--}12000 \text{ km s}^{-1}$, with $n_{II} = 25$.

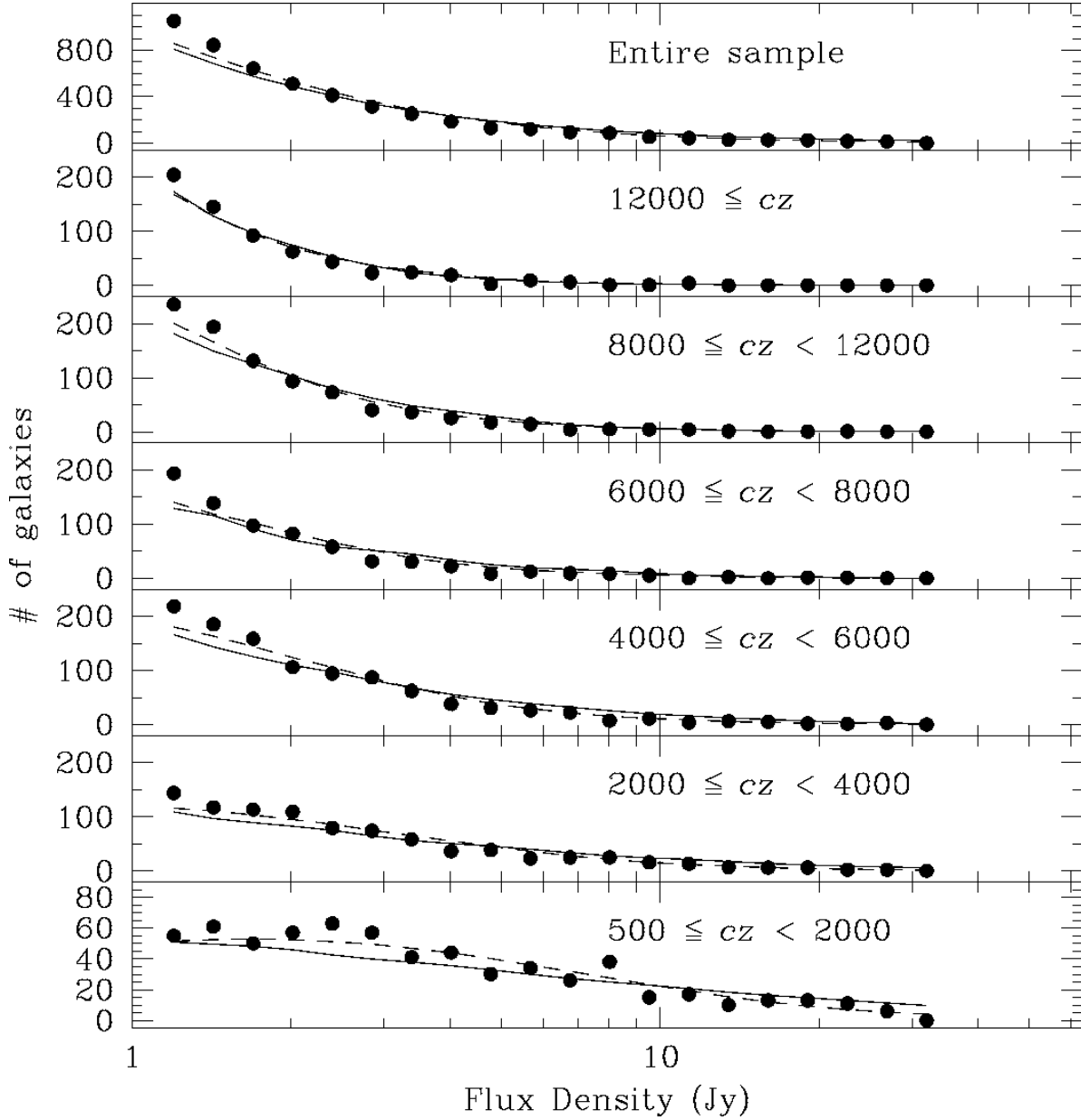


Fig. 5.— As in Fig. 4, but the luminosity functions are calculated with the SNWZ binning for both $p = 1$ and $p = 2$. Note that neither curve is a particularly good fit to the data, especially at the faint end, although $p = 2$ does somewhat better.

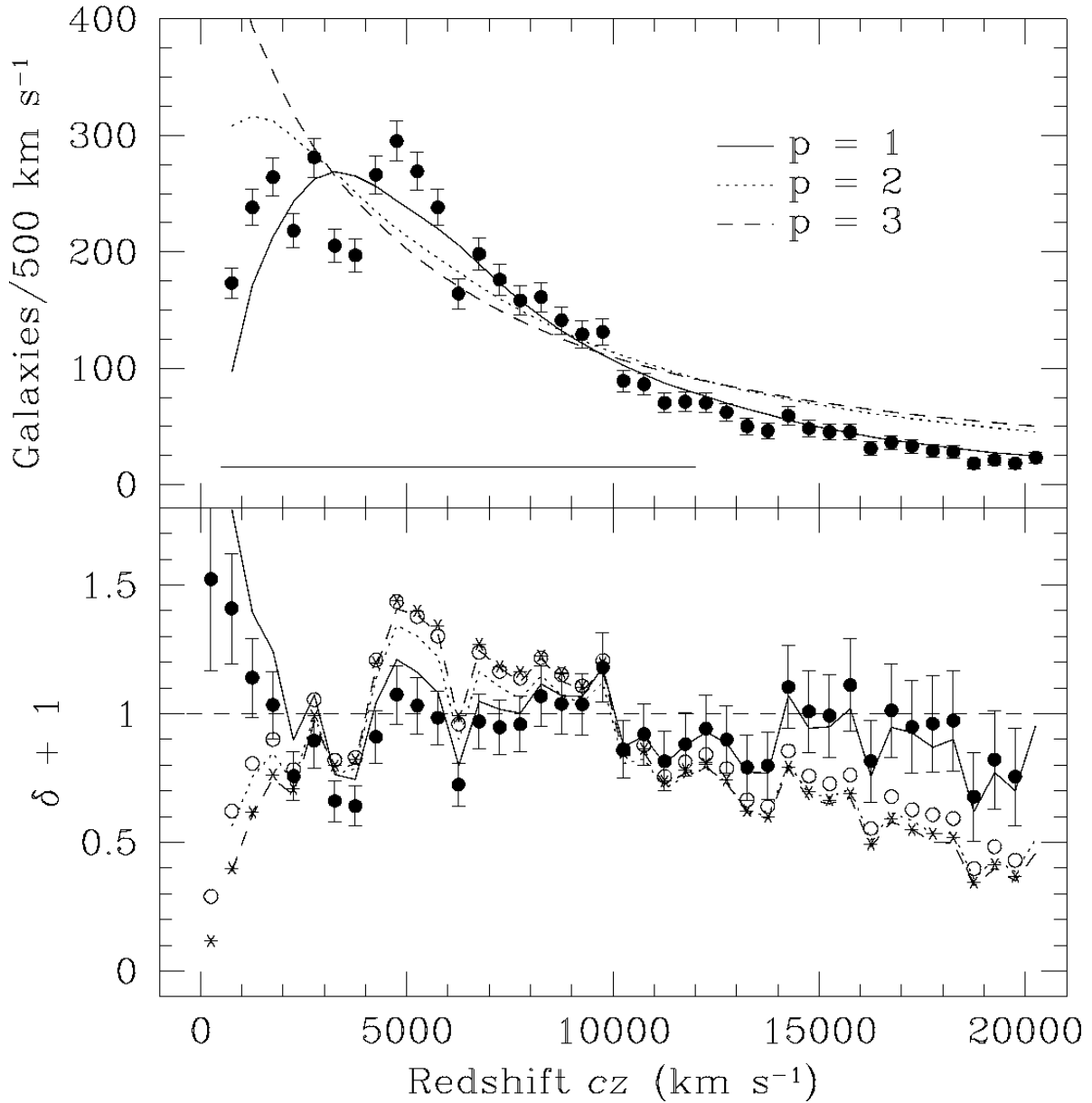


Fig. 6.— The upper panel shows the observed (points) and predicted (curves) distribution of galaxies with redshift for $p = 1, 2, 3$. The bottom panel shows the ratio of observed to predicted counts per bin; the predictions are based on the nonparametric luminosity function. The bar in the top panel marks the range of redshifts used in fitting the luminosity function. The points in the lower panel show the density field calculated nonparametrically and independently of the luminosity function, following Saunders *et al.* (1990). Solid points are for $p = 1$, open circles for $p = 2$, and stars are for $p = 3$. Error bars are shown only for $p = 1$ to keep the figure from getting too cluttered; however, the errors are quite insensitive to the value of p .

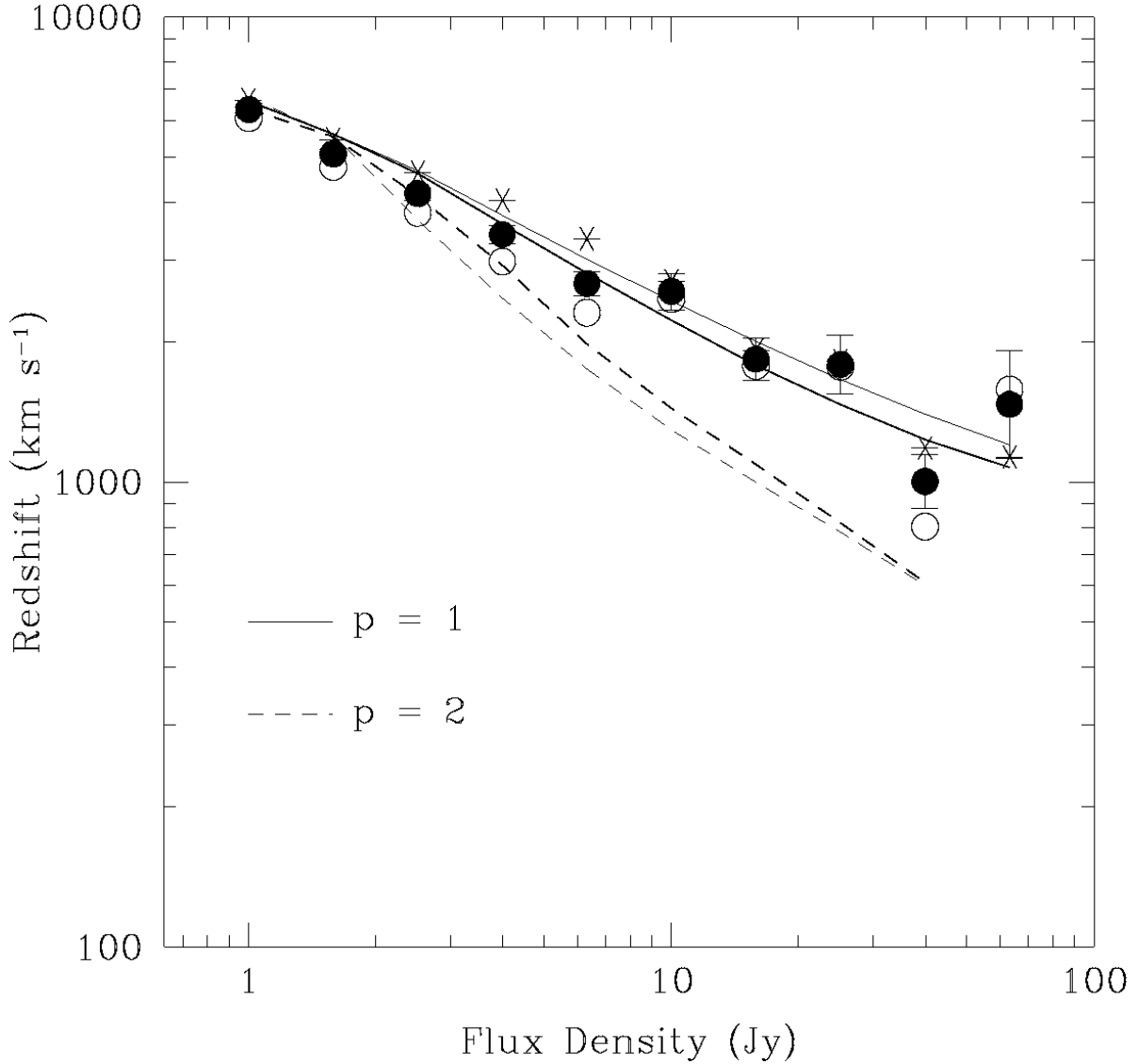


Fig. 7.— The solid points give the mean log redshift of galaxies in bins of log flux density from the entire *IRAS* 1.2 Jy sample, averaging over galaxies with redshifts between 500 and 20,000 km s⁻¹. The error bars are the error in the mean (that is, the standard deviation divided by the square root of the number of points in each bin). The open circles are the mean log redshift for galaxies in the Northern Galactic Hemisphere, while the stars are for the Southern Galactic Hemisphere. The light solid line gives the expected curve assuming $p = 1$ and a homogeneous universe, while the light dashed line assumes $p = 2$. The heavy solid and dashed lines give the expected density field taking into account the density field found non-parametrically in Fig. 6.

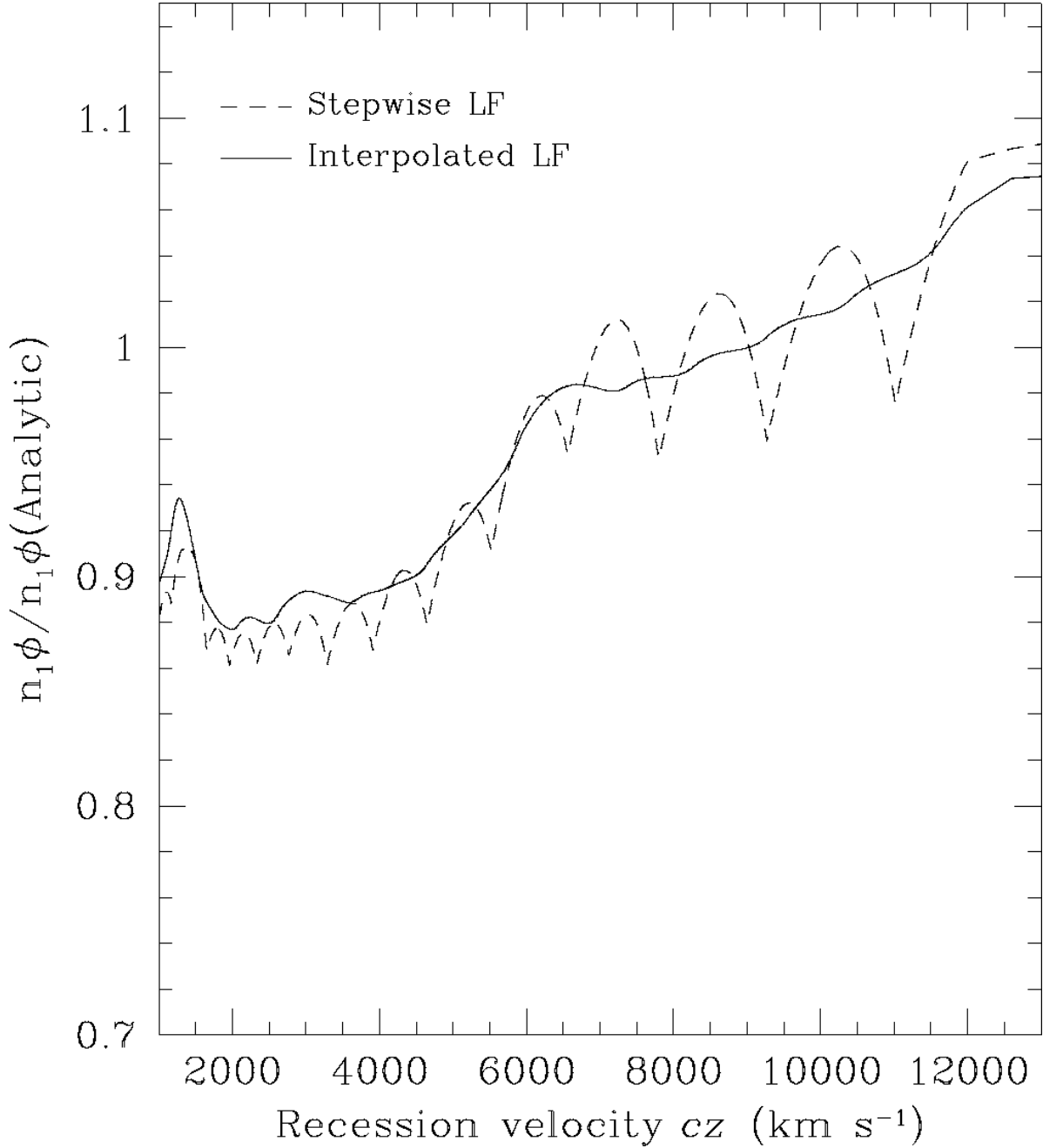


Fig. 8.— The solid line shows the ratio of the normalized selection function $n_1\phi(z)$ calculated from the interpolated luminosity function described in the Appendix, to that for the analytic luminosity function of Eqs. (10) and (11). The dashed line is the ratio of $n_1\phi(z)$ for the stepwise luminosity function to that of the analytic luminosity function. Notice the scalping in the latter.